Damage Management of Concrete Structures with Engineered Cementitious Materials and Natural Fibers: A Review of Potential Uses

Classical, Refined and Component-Wise Analysis of Reinforced-Shell Wing Structures

E. Carrera[1], A. Pagani[2], and M. Petrolo[3]
Politecnico di Torino, Corso Duca degli Abruzzi 24, 10129 Torino, Italy

This paper compares early and very recent approaches to the static analysis of reinforced-shell wing structures. Early approaches were those based on the pure *semimonocoque* theory along with beam assumptions of the Euler-Bernoulli and Timoshenko type. The recent approaches are based on a hierarchical, one-dimensional (1D) formulation. These are obtained by adopting various polynomial expansions of the displacement field above the cross-section of the structure according to the Unified Formulation (UF) which was recently proposed by the first author. Two classes were developed in the UF framework: (1) In the first class we developed Taylor Expansion (TE) models which exploit N-order Taylor-like polynomials; classical beam theories (Euler-Bernoulli and Timoshenko) were obtained as special cases of TE. (2) In the second class Lagrange Expansion (LE) models were built by means of four- (L4) and nine-point (L9) Lagrange-type polynomials over the cross-section of the wing. Component-wise (CW) approach was obtained by using different L4 and L9 descriptions for different wing components including panels, ribs, spar caps, stringers and transverse ribs. The finite element method was used to develop numerical applications in the weak form. Finite element matrices and vectors are expressed in terms of fundamental nuclei whose forms do not formally depend on the order and the expansion. A number of typical aeronautical structures were analyzed and *semimonocoque* results were compared to classical (Euler-Bernoulli and Timoshenko), refined (TE) and *component-wise* (LE) models. Stress and

---

[1] Professor of Aerospace Structures and Aeroelasticity, Department of Mechanical and Aerospace Engineering, erasmo.carrera@polito.it. Member AIAA, Corresponding Author.
[2] PhD student, Department of Mechanical and Aerospace Engineering, alfonso.pagani@polito.it.
[3] Research assistant, Department of Mechanical and Aerospace Engineering, marco.petrolo@polito.it.

displacement fields of simple statically determinate, redundant and open section wing-box structures were analyzed. Finite element models by a commercial software that make use of solid and shell elements were used for comparison purposes. Results have highlighted the enhanced capabilities of the present refined and *component-wise* formulations. The present Component-Wise approach appears the natural tool to analyze wing structures, as it leads to results that can only be obtained by use of 3D elasticity (solid) elements whose costs are at least one-order of magnitude higher than CW cases. CW models in conjunction with FE could be seen as a modern way of analyzing reinforced shell structures by removing classical assumptions of constant shear in the spar webs and panels.

Nomenclature

$\tilde{C}_{ij}$	= material coefficients
$\tilde{\boldsymbol{C}}_{pp}$, $\tilde{\boldsymbol{C}}_{pn}$, $\tilde{\boldsymbol{C}}_{np}$, $\tilde{\boldsymbol{C}}_{nn}$	= material stiffness subarrays
$\boldsymbol{D}_p$, $\boldsymbol{D}_{np}$, $\boldsymbol{D}_{ny}$	= differential operator matrices
E	= Young's modulus
F_s	= cross-section function of the variation
F_τ	= cross-section function of the variable
G	= shear modulus
$\boldsymbol{K}^{ij\tau s}$	= fundamental nuclei of stiffness matrix
L	= dimension of the structure in the y direction
L_{ext}	= external work
L_{int}	= internal work
N	= order of the expansion above the cross-section for the TE models
N_i	= shape function of the variable
N_j	= shape function of the variation
$\boldsymbol{q}$	= nodal displacement vector

$\boldsymbol{u}$ = displacement vector

u_x, u_y, u_z = displacement components in the x, y, and z directions

x, y, z = coordinates reference system

δ = virtual variation

$\boldsymbol{\epsilon}$ = strain vector

ν = Poisson's ratio

$\boldsymbol{\sigma}$ = stress vector

Ω = cross-section domain

I. Introduction

Primary aircraft structures are essentially reinforced thin shells [1]. These are so-called *semi-monocoque* constructions which are obtained by assembling three main components: skins (or panels), longitudinal stiffening members (including spar caps) and transversal stiffeners (ribs). The determination of stress/strain fields in these structural components is of prime interest for structural analysts. Many different approaches were developed in the first half of the last century. These are discussed in major reference books [1, 2] and more recently in [3]. Among these approaches the so-called Pure Semimonocoque (PS) (or "idealized semimonocoque") is the most popular, since it assumes constant shear into panels and shear webs. The main advantage of PS is that it leads to a system of linear algebraical equations. However the number of such equations rapidly increases for multi-bay box structures with high redundancy. The number of resulting equations (and redundancy) can be strongly reduced by coupling PS with assumptions from Euler-Bernoulli (Euler-Bernoulli Beam Theory, EBBT) or Timoshenko theories (Timoshenko Beam Theories, TBT). Many works are known to overcome limitations related to constant shear hypotheses, see [4–8] as examples. The systematic use of matrix methods in aircraft structure analysis was introduced by Argyris and Kensley [9]. Here, the PS approach and force methods were used to describe an automatic technique to build compliance matrices. This automatic technique is one of the pioneering contributions to the development of finite element methods (FEM).

Due to the advent of computational methods, mostly FEM, the analysis of complex aircraft

structures continued to be made using a combination of solids (3D), plates/shells (2D) and beams (1D). These were implemented first in NASTRAN codes. Many others commercial FE codes have been developed and used in aerospace industries. Nowadays FEM models with a number of unknowns (degrees of freedom, DOFs) close to 10^6 are widely used in common practise. The possible manner in which stringers, spar caps, spar webs, panels, ribs are introduced into FE mathematical models is part of the knowledge of structural analysts. A short discussion of this follows. A number of works have shown the necessity for a proper simulation of the stiffeners-panel "linkage". Satsangi and Murkhopadhyay [10] used 8-node plate elements assuming the same displacement field for stiffeners and plates. Kolli and Chandrashekhara [11] formulated an FE model with 9-node plate and 3-node beam elements. Gangadhara [12] carried out linear static analyzes of composite laminated shells using a combination of 8-node plate elements and 3-node beam elements. Recently, Thinh and Khoa [13] have developed a new 9-node rectangular plate model to study the free vibrations of shell structures with arbitrary oriented stiffeners. It is often necessary to model stiffeners out of the plate/shell element plane. In this case beam nodes are connected to the shell element nodes via rigid fictitious links. This methodology presents some inconsistencies. The main problem is that the out-of-plane warping displacements in the stiffener section are neglected and the beam torsional rigidity is not correctly predicted. Several solutions have been proposed in the literature to overcome this issue. Patel et al. [14] introduced a torsion correction factor. Vörös [15, 16] proposed a procedure to model the connection between the plate/shell and the stiffener where the shear deformation of the beam is neglected and the formulation of the stiffener is based on the well-known *Bernoulli-Vlasov* [17] theory. In Vörös' method the stiffener element has two nodes with seven degrees of freedom per node. In order to maintain the displacement compatibility between the beam and the stiffened element, a special transformation was used, which included torsional-bending coupling and the eccentricity of internal forces between the stiffener and the plate elements. 3D finite element models are usually implemented as soon as the wing's structural layouts are determined. Because of their complexity, solid models are commonly used only within optimization procedures. In fact, despite the availabilities of even cheaper computer power, these FEM models present large computational costs and their use in a multi-field iterative process, such as in an aeroelastic analysis, is quite a

burden. Nowadays the trend is to use equivalent, simplified, lower fidelity 1D FEM models (the so-called "stick-model") of the wing structure to be used within iterative algorithms. There are numerous papers dealing with wing stick models in the literature, such as [18–20]. These methodologies are based on the extraction of the structural stiffness of the wing with respect to its principal axes. Those stiffness properties are then employed to generate the wing stick model. Simplified models are generally created along the wing's elastic axis. This applies a geometrical constraint so that the stick model principal torsional axis act as the wing elastic axis. It could be concluded that the development of computationally cheaper models compared to those by standard FE models, but with high accuracy, still plays a crucial role in aircraft structure analysis.

The present work falls in the framework of the Carrera Unified Formulation, CUF, which has been developed during the last decade by the first author and his co-workers. CUF was initially devoted to the development of refined plate and shell theories, see [21, 22]. In recent works [23, 24], CUF has been extended to beam modeling. Two classes of CUF 1D models were proposed: the Taylor-expansion class, hereafter referred to as TE, and the Lagrange-expansion class, hereafter referred to as LE. TE models exploit N-order Taylor-like polynomials to define the displacement field above the cross-section with N as a free parameter of the formulation. Static [25, 26] and free-vibration analyzes [27, 28] showed the strength of CUF 1D models in dealing with arbitrary geometries, thin-walled structures and local effects. Moreover, asymptotic-like analyzes leading to reduced refined models were carried out [29]. The Euler-Bernoulli (EBBT) and Timoshenko (TBT) classical beam theories are derived from the linear Taylor-type expansion. The LE class is based on Lagrange-like polynomials to discretize the cross-section displacement field. LE models have only pure displacement variables. Static analyzes on isotropic [30] and composite structures [31] revealed the strength of LE models in dealing with open cross-sections, arbitrary boundary conditions and obtaining Layer-Wise descriptions of the 1D model.

The present paper proposes CUF-based approach in the analysis of complex wing structures. A number of significant problems dealing with reinforced-shell structures are addressed in the following sections. Classical, refined and *component-wise* (CW) models are implemented for different structural configurations. Particular attention is given to the CW approach. 'Component-wise' means

that each typical component of a reinforced-shell structure (i.e. stringers, sheet panels and ribs) can be modelled by means of a unique 1D formulation. The CW approach has recently been exploited for the analysis of laminated composites [32] and it has proven to be able to model single fibers and related matrices, entire layers and whole multilayers. In the present work the CW approach is presented as a efficient way of dealing with analysis of reinforced-shell wing structures.

The paper is organized as follows: a brief description of the models adopted is given in Section II; advanced beam theories based on CUF are described in Section III, together with the finite element formulation; numerical results are provided in Section IV; main conclusions are then outlined in Section V.

II. Description of the considered Structural Models

A brief description of the models used in the present paper is herein provided. Firstly analytical Pure Semimonocoque approaches are drawn. Refined and CW as well as classical beam theories are then introduced by means of 1D CUF, which is described in Section III.

A. Pure Semimonocoque (PS)

These models are based on the simplifying assumptions of the *semimonocoque* assembled components, as described in the Section I. Stringers are here considered as concentrated areas carrying only axial stresses, while webs and panels carry only shearing stresses. According to [1–3] the internal loads in a statically determinate reinforced-shell structure can be found by the use of static equilibrium equations alone. In a statically indeterminate structure, additional equations along with the static equilibrium equations are necessary to find all the internal stresses. In such a case we should impose compatibility conditions in order to deal with redundant forces and stresses. These conditions can be written in various forms by applying elasticity theorems; among these the Principle of Virtual Displacements (PVD) is used in this article as in [2, 3]. This approach is hereafter referred to as the PS (Pure *Semimonocoque*) model.

B. Beam Semimonocoque (BS)

The classical and best-known beam theories are EBBT [33] and TBT [34]. The former does not account for transverse shear deformations. The latter foresees a uniform shear distribution along the cross-section of the beam. For instance, referring to the coordinate frame shown in Fig. 1, the displacement components given by TBT can be written as:

$$\begin{aligned} u_x &= u_{x_1} \\ u_y &= u_{y_1} + x\ u_{y_2} + z\ u_{y_3} \\ u_z &= u_{z_1} \end{aligned} \tag{1}$$

where the parameters on the right hand sides (u_{x_1}, u_{y_1}, u_{z_1}, u_{y_2}, u_{y_3}) are the displacements and the rotations on the reference axis. EBBT requires a further condition, which results in the penalization of the shear strain components, ϵ_{xy} and ϵ_{zy}.

If EBBT is applied to the idealized *semimonocoque* assumptions it is possible to reduce redundancy in statically indeterminate structures. This method, hereafter referred to as BS (Beam *Semimonocoque*) model, is certainly less accurate than PS since more assumptions are required. It should be noted that for statically determinate structures the two methods coincide.

C. Refined Beam Models based on Taylor-Expansion (TE)

Several higher-order beam models can be found in open literature to overcome planar conditions on the displacement field over the wing cross-section. The Taylor-based CUF can be adopted to refine the displacement field of classical 1D models by adding expansion terms in Eq. (1). For instance, the TE second-order ($N = 2$) refined 1D model presents the following kinematic model

$$\begin{aligned} u_x &= u_{x_1} + x\ u_{x_2} + z\ u_{x_3} + x^2\ u_{x_4} + xz\ u_{x_5} + z^2\ u_{x_6} \\ u_y &= u_{y_1} + x\ u_{y_2} + z\ u_{y_3} + x^2\ u_{y_4} + xz\ u_{y_5} + z^2\ u_{y_6} \\ u_z &= u_{z_1} + x\ u_{z_2} + z\ u_{z_3} + x^2\ u_{z_4} + xz\ u_{z_5} + z^2\ u_{z_6} \end{aligned} \tag{2}$$

The 1D model described by Eq. 2 has 18 generalized displacement variables: three constant, six linear, and nine parabolic terms. The possibility of refining 1D models permits us to deal with a

wide variety of problems with no need for *ad hoc* formulations. Non-classical effects (e.g. warping, in-plane deformations, shear effects, bending-torsion couplings) are accounted for by opportunely varying the order of the adopted model. More details about TE models can be found in Section III and in the book by Carrera et al. [24].

D. Component-Wise (CW)

In a wing structural analysis, each component (e.g. ribs, stringers, panels, etc.) is commonly modelled through different elements (e.g. beams, shells, solids, etc.). For instance, by considering a simplified wing-box (see Fig. 2), stringers are considered as beams, whereas panels and ribs are modelled with 2D plate elements. 3D elasticity elements could be also used for stringers or for both stringers and panels. In the present paper, 1D LE elements were used to simultaneously model all the wing components. In a finite element framework this means that spar caps, webs, panels and ribs are modelled by means of the same 1D finite element and, therefore, with no need of ad hoc formulations for each component. More details about the LE beam theory and the implementation of CW models can be found in Section III.

III. CUF 1D Formulation

In this Section a brief description of models based on CUF is provided. First, some notations are introduced. Then TE and LE models are described. In Section III C the higher-order finite elements are formulated. Finally, in Section III D the use of the LE 1D elements in CW models is discussed.

A. Preliminaries

Referring to the coordinate frame shown in Fig. 1, let us introduce the transposed displacement vector,

$$\mathbf{u}(x,y,z) = \left\{ \begin{array}{ccc} u_x & u_y & u_z \end{array} \right\}^T \tag{3}$$

The cross-section of the structure is Ω, and the beam boundaries over y are $0 \leq y \leq L$. The stress, $\boldsymbol{\sigma}$, and strain, $\boldsymbol{\epsilon}$, components are grouped as follows:

$$\begin{aligned} \boldsymbol{\sigma}_p &= \left\{ \begin{array}{ccc} \sigma_{zz} & \sigma_{xx} & \sigma_{zx} \end{array} \right\}^T, \quad \boldsymbol{\epsilon}_p = \left\{ \begin{array}{ccc} \epsilon_{zz} & \epsilon_{xx} & \epsilon_{zx} \end{array} \right\}^T \\ \boldsymbol{\sigma}_n &= \left\{ \begin{array}{ccc} \sigma_{zy} & \sigma_{xy} & \sigma_{yy} \end{array} \right\}^T, \quad \boldsymbol{\epsilon}_n = \left\{ \begin{array}{ccc} \epsilon_{zy} & \epsilon_{xy} & \epsilon_{yy} \end{array} \right\}^T \end{aligned} \tag{4}$$

The subscript "n" stands for terms lying on the cross-section, while "p" stands for terms lying on planes which are orthogonal to Ω. In the case of small displacements with respect to a characteristic dimension of Ω, linear strain - displacement relations can be used

$$\begin{aligned} \boldsymbol{\epsilon}_p &= \boldsymbol{D}_p \mathbf{u} \\ \boldsymbol{\epsilon}_n &= \boldsymbol{D}_n \mathbf{u} = (\boldsymbol{D}_{n\Omega} + \boldsymbol{D}_{ny}) \mathbf{u} \end{aligned} \tag{5}$$

where $\boldsymbol{D}_p$ and $\boldsymbol{D}_n$ are linear differential operators,

$$\boldsymbol{D}_p = \begin{bmatrix} 0 & 0 & \frac{\partial}{\partial z} \\ \frac{\partial}{\partial x} & 0 & 0 \\ \frac{\partial}{\partial z} & 0 & \frac{\partial}{\partial x} \end{bmatrix}, \quad \boldsymbol{D}_{n\Omega} = \begin{bmatrix} 0 & \frac{\partial}{\partial z} & 0 \\ 0 & \frac{\partial}{\partial x} & 0 \\ 0 & 0 & 0 \end{bmatrix}, \quad \boldsymbol{D}_{ny} = \begin{bmatrix} 0 & 0 & \frac{\partial}{\partial y} \\ \frac{\partial}{\partial y} & 0 & 0 \\ 0 & \frac{\partial}{\partial y} & 0 \end{bmatrix} \tag{6}$$

Constitutive laws were exploited to obtain stress components,

$$\boldsymbol{\sigma} = \boldsymbol{C} \boldsymbol{\epsilon} \tag{7}$$

According to Eq.s (4), Eq. (7) becomes

$$\begin{aligned} \boldsymbol{\sigma}_p &= \tilde{\boldsymbol{C}}_{pp} \boldsymbol{\epsilon}_p + \tilde{\boldsymbol{C}}_{pn} \boldsymbol{\epsilon}_n \\ \boldsymbol{\sigma}_n &= \tilde{\boldsymbol{C}}_{np} \boldsymbol{\epsilon}_p + \tilde{\boldsymbol{C}}_{nn} \boldsymbol{\epsilon}_n \end{aligned} \tag{8}$$

In the case of isotropic material the matrices $\tilde{\boldsymbol{C}}_{pp}$, $\tilde{\boldsymbol{C}}_{nn}$, $\tilde{\boldsymbol{C}}_{pn}$, and $\tilde{\boldsymbol{C}}_{np}$ are

$$\tilde{\boldsymbol{C}}_{pp} = \begin{bmatrix} \lambda+2G & \lambda & 0 \\ \lambda & \lambda+2G & 0 \\ 0 & 0 & G \end{bmatrix}, \quad \tilde{\boldsymbol{C}}_{nn} = \begin{bmatrix} G & 0 & 0 \\ 0 & G & 0 \\ 0 & 0 & \lambda+2G \end{bmatrix}, \quad \tilde{\boldsymbol{C}}_{pn} = \tilde{\boldsymbol{C}}_{np}^{T} = \begin{bmatrix} 0 & 0 & \lambda \\ 0 & 0 & \lambda \\ 0 & 0 & 0 \end{bmatrix} \tag{9}$$

where G and λ are the Lamé's parameters. If Poisson ν and Young E moduli are used one has $G = \frac{E}{(2(1+\nu)}$ and $\lambda = \frac{\nu E}{((1+\nu)(1-2\nu))}$. Additional details can be found in [35] and [36].

B. One-dimensional advanced formulation with variable (hierarchial) kinematics

In the framework of the CUF, the displacement field above the cross-section is the expansion of generic functions, F_τ,

$$\mathbf{u}(x,y,z) = F_\tau(x,z)\mathbf{u}_\tau(y), \qquad \tau = 1,2,....,M \tag{10}$$

where F_τ vary over the cross-section. $\mathbf{u}_\tau$ is the displacement vector and M stands for the number of terms of the expansion. According to the Einstein notation, the repeated subscript, τ, indicates summation. The choice of F_τ determines the class of 1D CUF model that has to be adopted. Two cases are addressed in this paper: TE and LE.

TE 1D models are based on polynomial expansions, $x^i\ z^j$, of the displacement field above the cross-section of the structure, where i and j are positive integers. A generic N-order displacement field is therefore expressed by

$$\mathbf{u} = \sum_{N_i=0}^{N} \left(\sum_{M=0}^{N_i} x^{N-M}\ z^M\ \mathbf{u}_{\frac{N(N+1)+M+1}{2}} \right) \tag{11}$$

Eq. (2) is a particular case of Eq. (11). The order N of the expansion is arbitrary and defines the beam theory. N is set as an input of the analysis. The choice of N, for a given structural problem, is usually made through a convergence study.

The refined TE models described above are characterized by degrees of freedom (displacements and N-order derivatives of displacements) with a correspondence to the axis of the beam (see Fig.

3). The expansion can also be made by using only pure displacement values, e.g. by using Lagrange polynomials. The LE class exploits Lagrange-like polynomials to build 1D higher-order models. In this work, two types of cross-section polynomial sets were adopted: four-point elements, L4, and nine-point elements, L9. The isoparametric formulation was exploited to deal with arbitrary shaped geometries. The L4 interpolation functions are given in [37],

$$F_\tau = \frac{1}{4}(1 + r\ r_\tau)(1 + s\ s_\tau) \qquad \tau = 1, 2, 3, 4 \tag{12}$$

where r and s vary from -1 to $+1$, whereas r_τ and s_τ are the coordinates of the four points whose numbering and location in the natural coordinate frame are shown in Fig. 4a. In the case of an L9 element the interpolation functions are given by

$$F_\tau = \tfrac{1}{4}(r^2 + r\ r_\tau)(s^2 + s\ s_\tau) \qquad \tau = 1, 3, 5, 7$$

$$F_\tau = \tfrac{1}{2}s_\tau^2(s^2 - s\ s_\tau)(1 - r^2) + \tfrac{1}{2}r_\tau^2(r^2 - r\ r_\tau)(1 - s^2) \qquad \tau = 2, 4, 6, 8 \tag{13}$$

$$F_\tau = (1 - r^2)(1 - s^2) \qquad \tau = 9$$

The nine points of the L9 element are shown in Fig. 4b. For instance, the displacement field given by an L4 element is

$$\begin{aligned} u_x &= F_1\ u_{x_1} + F_2\ u_{x_2} + F_3\ u_{x_3} + F_4\ u_{x_4} \\ u_y &= F_1\ u_{y_1} + F_2\ u_{y_2} + F_3\ u_{y_3} + F_4\ u_{y_4} \\ u_z &= F_1\ u_{z_1} + F_2\ u_{z_2} + F_3\ u_{z_3} + F_4\ u_{z_4} \end{aligned} \tag{14}$$

where $u_{x_1}, ..., u_{z_4}$ are the displacement variables of the problem and represent the translational displacement components of each of the four points of the L4 element. The adopted cross-section displacement field (L4 or L9) defines the beam theory. For further refinements, the cross-section can be discretized by using several L-elements as in Fig. 3b-d. More details about LE models can be found in the paper by Carrera and Petrolo [30].

C. FE Formulation based on LE and TE

The FE approach was adopted to discretize the structure along the y-axis. This process is conducted via a classical finite element technique, where the displacement vector is given by

$$\mathbf{u}(x, y, z; t) = F_\tau(x, z) N_i(y) \mathbf{q}_{\tau i}(t) \tag{15}$$

N_i stands for the shape functions and $\mathbf{q}_{\tau i}$ for the nodal displacement vector,

$$\mathbf{q}_{\tau i} = \left\{ \begin{array}{ccc} q_{u_{x_{\tau i}}} & q_{u_{y_{\tau i}}} & q_{u_{z_{\tau i}}} \end{array} \right\}^T \tag{16}$$

For the sake of brevity, the shape functions are not reported here. They can be found in many books, for instance in [38]. Elements with four nodes (B4) were adopted in this work, that is, a cubic approximation along the y axis was assumed. The choice of the cross-section discretization for the LE class (i.e. the choice of the type, the number and the distribution of cross-section elements) or the theory order, N, for the TE class is completely independent of the choice of the beam finite element to be used along the axis of the beam.

The stiffness matrix of the elements and the external loadings vector were obtained via the PVD

$$\delta L_{int} = \int_V (\delta \boldsymbol{\epsilon}_p^T \boldsymbol{\sigma}_p + \delta \boldsymbol{\epsilon}_n^T \boldsymbol{\sigma}_n) dV = \delta L_{ext} \tag{17}$$

where L_{int} stands for the strain energy, L_{ext} is the work of the external loadings and δ stands for the virtual variation. The virtual variation of the strain energy was rewritten using Eq.s (5), (8), (10) and (15):

$$\delta L_{int} = \delta \mathbf{q}_{\tau i}^T \mathbf{K}^{ij\tau s} \mathbf{q}_{sj} \tag{18}$$

where $\mathbf{K}^{ij\tau s}$ is the stiffness matrix in the form of the fundamental nucleus. In a compact notation,

it can be written as:

$$
\begin{aligned}
\boldsymbol{K}^{ij\tau s} = & \overset{ij}{I_l} \triangleleft \left(\boldsymbol{D}_{np}^T F_\tau \boldsymbol{I}\right)\Big[\tilde{\boldsymbol{C}}_{np}\left(\boldsymbol{D}_p F_s \boldsymbol{I}\right) + \tilde{\boldsymbol{C}}_{nn}\left(\boldsymbol{D}_{np} F_s \boldsymbol{I}\right)\Big] + \\
& \left(\boldsymbol{D}_p^T F_\tau \boldsymbol{I}\right)\Big[\tilde{\boldsymbol{C}}_{pp}\left(\boldsymbol{D}_p F_s \boldsymbol{I}\right) + \tilde{\boldsymbol{C}}_{pn}\left(\boldsymbol{D}_{np} F_s \boldsymbol{I}\right)\Big] \triangleright_\Omega + \\
& I_l^{ij,_y} \triangleleft \Big[\left(\boldsymbol{D}_{np}^T F_\tau \boldsymbol{I}\right)\tilde{\boldsymbol{C}}_{nn} + \left(\boldsymbol{D}_p^T F_\tau \boldsymbol{I}\right)\tilde{\boldsymbol{C}}_{pn}\Big] F_s \triangleright_\Omega \boldsymbol{I}_{\Omega y} + \\
& I_l^{i,_y j} \boldsymbol{I}_{\Omega y} \triangleleft F_\tau \Big[\tilde{\boldsymbol{C}}_{np}\left(\boldsymbol{D}_p F_s \boldsymbol{I}\right) + \tilde{\boldsymbol{C}}_{nn}\left(\boldsymbol{D}_{np} F_s \boldsymbol{I}\right)\Big] \triangleright_\Omega + \\
& I_l^{i,_y j,_y} \boldsymbol{I}_{\Omega y} \triangleleft F_\tau \tilde{\boldsymbol{C}}_{nn} F_s \triangleright_\Omega \boldsymbol{I}_{\Omega y}
\end{aligned}
\tag{19}
$$

where:

$$
\boldsymbol{I}_{\Omega y} = \begin{bmatrix} 0 & 1 & 0 \\ 1 & 0 & 0 \\ 0 & 0 & 1 \end{bmatrix} \qquad \triangleleft \ldots \triangleright_\Omega = \int_\Omega \ldots \, d\Omega \tag{20}
$$

$$
\left(\overset{ij}{I_l}, I_l^{ij,_y}, I_l^{i,_y j}, I_l^{i,_y j,_y}\right) = \int_l \left(N_i N_j,\, N_i N_{j,_y},\, N_{i,_y} N_j,\, N_{i,_y} N_{j,_y}\right) dy \tag{21}
$$

It should be noted that $\mathbf{K}^{ij\tau s}$ does not depend either on the expansion order or on the choice of the F_τ expansion polynomials. These are the key-points of CUF which allows, with only nine FORTRAN statements, the implementation of any-order of multiple class theories.

The loadings vector which is variationally coherent to the model was derived for the case of a generic concentrated load $\mathbf{P}$ acting on the application point (x_p, y_p, z_p),

$$
\mathbf{P} = \left\{ \begin{array}{ccc} P_{u_x} & P_{u_y} & P_{u_z} \end{array} \right\}^T \tag{22}
$$

Any other loading condition can be similarly treated. The virtual work due to $\mathbf{P}$ is

$$
\delta L_{ext} = \mathbf{P} \delta \mathbf{u}^T \tag{23}
$$

The virtual variation of $\mathbf{u}$ in the framework of CUF has been introduced in Eq. (10), then

$$\delta L_{ext} = F_\tau \mathbf{P} \delta \mathbf{u}_\tau^T \tag{24}$$

By introducing the nodal displacements and the shape functions, Eq. (24) becomes

$$\delta L_{ext} = F_\tau N_i \mathbf{P} \delta \mathbf{q}_{\tau i}^T \tag{25}$$

where F_τ and N_i are evaluated in (x_p, z_p) and y_p respectively. The last equation permits the identification of the components of the nucleus which have to be loaded, that is, it permits the proper assembling of the loading vector by detecting the displacement variables that have to be loaded.

A detailed description of 1D formulations based on CUF can be found in the recent book by Carrera et al. [24].

D. CW models through 1D LE elements

The LE formulation was used in this paper to implement CW models of reinforced-shell wing structures, as shown in Fig. 5a where a two-stringer spar is considered. Figure 5b shows a possible CW model of the spar where each component was modelled via one 1D LE element. Each LE element is then assembled above the cross-section to obtain the global stiffness matrix based on the 1D formulation. Since panels could not be reasonably modelled via a 1D formulation, 1D CW models can be refined by using several L-elements for one component. This aspect is shown in Fig. 5c where the panel is modelled via two 1D LE elements. By exploiting the present 1D formulation, the analysis capabilities of a structural model can be enhanced by 1. locally refining the LE discretization; 2. using higher-order LE elements (e.g. 4-node, 9-node, 16-node, etc.).

IV. Numerical Results

The various approaches considered to wing structure analysis are evaluated in this section and compared to commercial FEM software results.

Two classical spars are considered for the first assessment. Then two more complex wing structures are analyzed to show the capability of the present CUF models of dealing with ribs and open sections. Unless otherwise stated, the results by refined and CW models are compared to 3D solid FEM models since the present models are not affected by the discontinuities in the displacement fields that may result from a combination of 1D, 2D, and 3D elements. TE and LE models are also compared with classical beam theories and analytical results by theories based on idealized stiffened-shell structures for further comparisons. Particular attention is given to the capabilities offered by CW models of dealing with thin-walled reinforced structures as well as with solid and shell-like FEM analyzes with significantly lower computational costs.

A. Two-Stringer Spar

The simplest spar structure shown in Fig. 6 was considered first. Stringers were taken to be rectangular for convenience, however their shape does not effect the validity of the proposed analysis. The geometrical data are as follows: axial length, $L = 3$ $[m]$; cross-section height, $h = 1$ $[m]$; area of the spar caps, $A_s = 0.9 \times 10^{-3}$ $[m^2]$; web thickness, $t = 1 \times 10^{-3}$ $[m]$. The whole structure is made of an aluminum alloy material. The material data are: the Young modulus, E=75 [GPa]; Poisson ratio, ν= 0.33. The beam was clamped at $y = 0$ and a point load, $F_z = -1 \times 10^4$ $[N]$, was applied at $[0, L, 0]$.

The vertical displacement, u_z, at the loaded point is reported in Table 1. Results were related to a MSC/NASTRAN© FE model with 8-node solid elements and to classical beam theories, EBBT and TBT. Refined theories related to higher-order TE models are also reported in Table 1. N refers to the expansion order of the TE beam theory. Component-Wise LE results are given. These models were obtained by using two different L9 cross-section distributions, as shown in Fig. 7. All the 1D CUF models were implemented by considering 10 B4 elements along the y-axis since this mesh offers good accuracy. A detailed analysis of the effects of the number and the type of finite elements along the beam axis can be found in [24]. The third column in Table 1 quotes the number of the degrees of freedom (DOFs) for each model. DOFs are used to estimate the computational efficiency of the proposed models. It should be noticed that another advantage given by 1D formulations is

that they can, in general, lead to lower stiffness-matrix bandwidths with respect to 2D or 3D FE mathematical models.

It should be noted that the CW FE approach uses only physical surfaces (the four faces of caps and the inner and outer surfaces of the panel) to build FE mathematical models. The FE models and the classical beam and plate/shell approaches usually introduce artificial surfaces and lines (e.g. the beam axis and the reference surface for shell elements). This characteristic of CW models is a unique feature that makes this approach advantageous in a CAE/CAD scenario.

The analytical results related to BS and PS approaches are provided and evaluated as follows (see [3]):

$$u_{z_{BS}} = \frac{F_z L^3}{3EI}, \qquad u_{z_{PS}} = \frac{F_z L^3}{3EI} + \frac{F_z L}{AG} \tag{26}$$

where I is the cross-section moment of inertia about the x-axis, G is the shear modulus and A is the overall cross-section area. In the present paper stress fields are evaluated in terms of axial loads in stringers and shear flows on panels/webs, in order to compare the results with classical analytical models. Table 2 reports the axial load in the upper stringer, P, at $y = 0$ and the mean shear flow in the panel, q, at $y = \frac{L}{2}$. In according with [3, chap. 6 p. 88], for both BS and PS analytical models, P and q were evaluated as

$$P = \frac{F_z L}{\overline{h}}, \qquad q = -\frac{F_z}{\overline{h}} \tag{27}$$

where $\overline{h}$ is the distance between the centers of the two stringers.

CUF and solid models are not affected by the generalization of the classical ideal reinforced-shell assumptions. For this reason, the shear flows acting on panels in 1D refined CUF models and in MSC/NASTRAN© models are not constant within the panels and are reported as mean shear flows, evaluated as

$$q_m = \frac{1}{l} \int_A \tau \, dA$$

Conversely, in both MSC/NASTRAN© and CUF models, P was computed by evaluating the constraint forces multiplying the non-constrained stiffness matrix by the displacement vector.

The variation in the axial stress and the shear stress versus the z-axis is presented in Fig.s 8. Results by SOLID, TE, LE and classical beam models are reported. A convergence study was carried out for MSC/NASTRAN© models and the results are shown in Table 3. The following considerations arise from the analyzes.

1. Refined beam theories, especially LE, allows us to obtain the results of the solid model (which is the most accurate and at the same time the most computationally expensive).

2. The number of degrees of freedom of the present models is significantly reduced with respect to the MSC/NASTRAN© solid model.

3. Both MSC/NASTRAN© and higher-order CUF models, unlike analytical theories based on idealized stiffened-shell structures and classical 1D models, highlight the fact that the axial stress component, σ_{yy} is not linear versus z and that the shear stress component, σ_{yz}, is not constant along the sheet panel.

4. The Component-Wise capability of the present LE approach is clearly evident from the conducted analysis.

B. Three-Stringer Spar

A longeron with three longitudinal stiffeners was subsequently considered. The geometry of the structure is shown in Fig. 9. The spar was clamped at $y = 0$, whereas a point load, F_z, was applied at the center of the upper stringer at $y = L$. The magnitude of F_z is equal to -1×10^4 $[N]$. The geometrical characteristics were as follows: axial length, $L = 3$ $[m]$; cross-section height, $h = 1$ $[m]$; area of the stringers, $A_s = 1.6 \times 10^{-3}$ $[m^2]$; sheet panel thickness, $t = 2 \times 10^{-3}$ $[m]$; distance from the intermediate stringer to the x-y plane, $b = 0.18$ $[m]$. The whole structure is made of the same isotropic material as in the previous case.

Table 4 shows the displacement, u_z, evaluated at the center of the intermediate stringer together with the indication of the number of degrees of freedom for each considered model. In the 1^{st} and

2^{nd} rows classical analytical models results are reported. The increasing order Taylor-type models are considered in rows 3 to 7. The CW LE model was obtained by discretizing the cross-section with 5 L9 elements, one for each spar component (stringers and webs), and the results are shown in row 7. The last row shows the solid model result obtained by an FE model in MSC/NASTRAN©. The SOLID model was obtained so that to guarantee a low aspect-ratio of the 8-node solid elements.

Table 5 shows the stress fields of the considered structure. Axial loads in the top (P_1), middle (P_2) and bottom (P_3) stringers are evaluated at $y = 0$, together with the mean shear flows on the upper (q_1) and bottom (q_2) sheet panels at $y = \dfrac{L}{2}$. Referring to the BS model, the axial loads in the stringers were evaluated by means of the Navier equation that gives the longitudinal normal stress distribution over the spar section. Considering a coordinate frame laying on the center of mass, the following equation holds,

$$P_{i_{BS}} = \frac{F_z L}{I} A_i Z_i \tag{28}$$

where P_i is the axial force in the i-th stringer, A_i the concentrated boom area and Z_i the vertical coordinate. The shear flows q_i were evaluated from the equilibrium equations. For the structural configuration analyzed, the PS differs from the BS solution. In fact, the three-stringer spar has one redundance (q_1 and q_2 consist of two independent unknowns along the z-axis which are related by only one common equilibrium equation). The PVD was employed to take into account the deformability of stringers and panels. Let X be the redundant force in the lower longitudinal. By using the formula in [3], one has:

$$X = \frac{\dfrac{E}{G}\Big(\dfrac{h_2}{h_1}\Big)\dfrac{1}{t} + \dfrac{2}{3}L^2\Big(\dfrac{h_2}{h_1^2} + \dfrac{1}{2h_1}\Big)\dfrac{1}{A}}{\dfrac{E}{G}\Big(\dfrac{h_2^2}{h_1^2} + \dfrac{h_2}{L}\Big)\dfrac{1}{t} + \dfrac{2}{3}L\Big(\dfrac{h_2^2}{h_1^2} + \dfrac{h_2}{h_1} + 1\Big)\dfrac{1}{A}} F_z \tag{29}$$

where h_1 is the distance between the top and the intermediate stringer, h_2 is the distance between the intermediate and the bottom stringer. The axial forces $P_{i_{PS}}$ and the shear flows $q_{i_{PS}}$ were

computed by substituting Eq. (29) in the equilibrium equations (for details see [3, chap. 8 p.168]).

$$\begin{aligned} P_{1_{PS}} &= -F_z\frac{L}{h_1} + X\frac{h_2}{h_1} \\ P_{2_{PS}} &= F_z\frac{L}{h_1} - X(1+\frac{h_2}{h_1}) \\ P_{3_{PS}} &= X \\ q_{1_{PS}} &= \frac{F_z}{h_1} - X\frac{h_2}{Lh_1} \\ q_{2_{PS}} &= X\frac{1}{L} \end{aligned} \tag{30}$$

The distribution of the axial stress, σ_{yy}, and the shear stress, σ_{yz} versus the z-axis are shown in Fig. 10. The following statements hold.

5. The 5 L9 model is very close to the solid solution with a significant reduction of computational costs.

6. Results from Taylor-type models are less accurate than those from CW models.

7. The classical models are totally inadequate for the detection of stress fields of the considered structural problems.

8. Even in this particular case the CW capability of the CUF-based LE approach is highly evident. Hence, the stress fields in the stringers/panels are described as accurately as those in the FE solids cases.

C. Rectangular Wing Box

A proper wing box both with and without a rib at the tip section (Fig. 11) was further analyzed. The length-to-width ratio, L/b, is equal to 3.125 with L as high as 3 $[m]$. The cross-section height, h, is equal to 0.46 $[m]$, whereas the thickness of the four sheet panels is $t = 2 \times 10^{-3}$ $[m]$. The area of the spar caps is $A_s = 1.6 \times 10^{-3}$ $[m^2]$. The wing box configuration with a rib at the tip presents a transversal stiffener with a thickness of $r = t$. The structure is made of the same isotropic material as in the previous cases. A point load, $F_z = -1 \times 10^4$ $[N]$, was applied at $[b, L, \frac{h}{2}]$.

First, a convergence study of the LE CW models was carried out. Table 6 shows the mean shear flows on the panels, the axial forces in the stringers and the number of degrees of freedom for both

CW and MSC/NASTRAN© models. Each CW model has a different number of LE elements on the panels. In particular, in the 8 L9 model stringers and panels were modelled with 1 L9 element each. In the 12 L9 model, one L9 element was used for each stringer and two elements were used for each panel. In the 20 L9 model, one L9 element was used for each stringer and four elements were used for each panel. The rib was discretized with a combination of L4 and L9 elements. The SOLID model was completely built with 8-node solid elements, while the SOLID/SHELL model was obtained as a combination of both solid and 4-node plate finite elements. Both stringers and rib were discretized by means of solid elements in the SOLID/SHELL model, whereas plate elements were used for skins and webs. q_1 and P_1 refer to the top panel and to the top right stringer respectively, q_2, q_3, q_4 and P_2, P_3, P_4 follow a clock-wise enumeration. It should be underlined that LE CW models, differently from TE, allow the local refinement of the components. For the structure considered, one L9 element was not sufficient to accurately detect the *shear lag* within the panel. Consequently, the axial forces in the stringers were not correct. The solution was enhanced by increasing the number of 1D L9 elements used to discretize the panel.

Table 7 quotes the mean shear flows on the panels, the axial forces in the stringers and the number of degrees of freedom for each implemented model. Results from both analytical methods and classical beam theories are reported. Rows 5 to 7 consider the TE models. Finally, the convergent solution by the CW method is given in row 8 and the MSC/NASTRAN© models are reported in the last two rows.

BS and PS models (but also classical beam theories) are not able to correctly detect the behavior of the no rib configuration of the rectangular wing box. In fact, one of the main assumptions of these methods is that the ribs are "rigid within their planes". The solutions provided by these methods for the wing box are described in the following. In accordance with the BS method, the axial forces and the shear flows were evaluated by solving firstly Eq. (28) and then the equilibrium equations. Conversely, as in the previous case, the PS solution requires the application of the PVD. Let X be

the redundant force applied in the bottom left stringer [3, chap. 10 p.196],

$$X = \frac{\frac{(b-h)}{4Gth}}{-\frac{4L}{3EA} - \frac{(b+h)}{2LGt}} F_z \tag{31}$$

Subsequently, PS stress fields were computed by substituting X in the equilibrium equations.

Deformed tip cross-sections of both configurations are shown in Fig. 12 and 13, together with variations in the shear stress components on the sheet panels. Confirming the previous remarks, the following further considerations can be made:

9. The results from the LE and MSC/NASTRAN© models coincide for both structural configurations. In particular, the results from the CW model of the un-ribbed box are more similar to those from the SOLID model than to those from the SOLID/SHELL model. This is most likely due to the discontinuities in the displacement fields on the panel-stringer interfaces that affect the SOLID/SHELL model.

10. For the wing-box considered, the results given by the eight-order ($N = 8$) TE model are not sufficiently accurate. An higher than eight-order TE model could be necessary to correctly detect the *shear-lag*. However, higher-order models imply a larger number of the degrees of freedom.

11. Classical beam models and the PS approach are not able to correctly describe the wing box model without the rib.

D. Three-Bay Wing Box

The last analysis case was carried out on the three-bay wing box for which PS and BS solutions were given in Rivello's book. The considered structure is shown in Fig. 14a [2, chap. 11 p. 301], whereas Fig.s 14b and c show its variations. These examples highlight the capability of the present advanced 1D models to accurately describe the effects due to ribs and open sections. The structures consist of three wing boxes each with a length, l, equal to 0.5 $[m]$. The cross-section is a trapezium with a height $b = 1$ $[m]$. The two webs of the spars have a thickness of 1.6×10^{-3} $[m]$, whereas $h_1 = 0.16$ $[m]$ and $h_2 = 0.08$ $[m]$. The top and the bottom panels have a thickness of 0.8×10^{-3}

$[m]$, as well as ribs. The area of the stringers is $A_s = 8 \times 10^{-4}$ $[m^2]$. The wing is completely made of an aluminium alloy 2024, having $G/E = 0.4$. The cross-section in $y = 0$ was clamped and a point load, $F_z = 2 \times 10^4$ $[N]$, was applied at $[b, 2 \times l, \frac{h_2}{2}]$.

Table 8 shows the vertical displacement values, u_z and the computational costs for each model. Results related to the CUF models are validated by an MSC/NASTRAN© model built both with solid and shell FE elements as discussed in the previous analysis. The CW models were obtained by using both L4 and L9 elements, as in the rectangular wing box.

Fig.s 15, 16 and 17 show the spanwise variation of the axial and the shear stress components for the three different configurations. BS and PS solutions are provided for the full model of the three-bay wing box for comparison. The structure has three redundancies. The PVD can be used to correct the BS solution. Let X_1, X_2 and X_3 be the redundant forces that must be added to the BS solution to obtain the true forces in the lower left stringer at a distance of 0, l and $2 \times l$ from the root. The redundant forces are calculated by means of the PVD. The following results hold:

$$X_1 = -36.446\ [N]; \qquad X_2 = -6.912\ [N]; \qquad X_3 = 13.908\ [N] \tag{32}$$

These values allow us to compute the axial forces and the shear flows for the PS method. For the complete resolution see [2, chap. 11 p. 301].

Finally, Table 9 reports the values of the stress components of both LE and SOLID/SHELL models. The following remarks can be made.

12. LE models correctly predict ribs and local effects, as match the results obtained with solid/shell models.

13. Higher than sixth-order TE models are required to correctly predict the cross-section deformability.

14. The PS method is quite accurate in the description of the full configuration of the three-bay wing box. Conversely, the BS method is not suitable as the structure is statically indeterminate.

V. Conclusions

This paper has considered and compared existing methods and recent approaches that exploit one-dimensional structural theories based on the Unified Formulation, which allows for the straightforward implementation of higher-order analysis without the need of extensive revisions of the model. Pure Semimonocoque analyses along with beam assumptions have been compared to refined and component-wise models and to shell and solid solutions obtained by a commercial FEM software.

As general guidelines and recommendations, it can be stated that TE should be used for global responses, such as displacements. On the other hand, CW models have to be adopted if local responses - such as stress, strains - are of interest. The main conclusion to be drawn is that the present component-wise analysis of reinforced shell structures appears to the authors as the most convenient way, in terms of both accuracy and computational costs, to capture the global and local (component-wise) physical behavior of wing structures. 3D FEM analysis is required to reach the same accuracy with a number of degrees of freedom at least one-order of magnitude higher than the present models. Additionally, the present CW approach allows us to build FE mathematical models by only using physical surfaces; artificial lines (beam axes) and surfaces (plate/shell reference surfaces) are no longer used.

References

[1] Bruhn, E. F., *Analysis and Design of Flight Vehicle Structures*, Tri-State Offset Company, 1973.

[2] Rivello, R. M., *Theory and analysis of flight structures*, McGraw-Hill, 1969.

[3] Carrera, E., *Fondamenti sul Calcolo di Strutture a Guscio Rinforzato per Veicoli Aerospaziali*, Levrotto & Bella, 2011.

[4] Cicala, P., "Sul Calcolo delle Strutture a Guscio," *L'Aerotecnica*, Vol. XXVI, No. 3, 1946, pp. 138–148, Part 1 of 4.

[5] Goodey, W. J., "A Stressed Skin Problem," *Aircr. Engin*, 1938.

[6] Ebner, H. and Koller, H., "Zur Berechnung des Kraftver laufes in versteiften Zylindershalen," *Luftf. Forschg.*, 1937.

[7] Ebner, H. and Koller, H., "Ueber den Kraftverlauf in längs und querversteiften Scheiben," *Luftf. Forschg.*, 1938.

[8] Broglio, L., *Introduzione di un metodo generale per il calcolo delle strutture a guscio*, Ist. poligr. dello Stato, Roma, 1952, Monografie scientifiche di aeronautica n. 1.

[9] Argyris, J. M. and Kelsey, S., *Energy theorems and structural analysis*, Butterworths, 1960.

[10] Satsangi, S. and Mukhopadhyay, M., "Finite element state analysis of girder bridges having arbitrary platform," *Int. Ass. of Bridge Struct. Engng.*, Vol. 17, 1987, pp. 65–94.

[11] Kolli, M. and Chandrashekhara, K., "Finite element analysis of stiffened laminated plates under transverse loading," *Composite Science and Technology*, Vol. 56, 1996, pp. 1355–1361.

[12] Gangadhara Prusty, B., "Linear static analysis of hat stiffened laminated shells using finite elements," *Finite elements in analysis and design*, Vol. 39, 2003, pp. 1125–1138.

[13] Thinh, T. I. and Khoa, N. N., "Free Vibration Analysis of Stiffened Laminated Plates Using a New Stiffened Element," *Technische Mechanik*, Vol. 28, No. 3–4, 2008, pp. 227–236.

[14] Patel, S. N., Datta, P. K., and Seikh, A. H., "Buckling and dynamic instability analysis of stiffened shell panels," *Thin-Walled Structures*, Vol. 44, 2006, pp. 321–333.

[15] Vörös, G. M., "A special purpose element for shell-beam systems," *Computers and Structures*, Vol. 29, No. 2, 1988, pp. 301–308.

[16] Vörös, G. M., "Finite element analysis of stiffened plates," *Periodica Polytechnica*, Vol. 51, No. 2, 2007, pp. 105–112.

[17] Vlasov, V. Z., *Thin-walled elastic beams*, National Science Foundation, Washington, 1961.

[18] Abdo, M., LâĂŹHeureux, R., Pepin, F., and Kafyeke, F., "Equivalent Finite Element Wing Structural Models Used for Aerodynamics-Structures Intraction," *CASI 16th Aerospace Structures and Materials Symposium*, Montreal, Quebec, April 2003.

[19] Piperni, P., Abdo, M., and Kafyeke, F., "The Building Blocks of Multi-Disciplinary Wing Design Method," *CASI 50th Annual General Meeting*, Montreal, Quebec, 2003.

[20] Elsayed, M. S. A., Sedaghati, R., and Abdo, M., "Accurate Stick Model Development for Static Analysis of Complex Aircraft Wing-Box Structures," *AIAA Journal*, Vol. 47, No. 9, 2009, pp. 2063–2075.

[21] Carrera, E., "Theories and finite elements for multilayered, anisotropic, composite plates and shells," *Archives of Computational Methods in Engineering*, Vol. 9, No. 2, 2002, pp. 87–140.

[22] Carrera, E., "Theories and finite elements for multilayered plates and shells: a unified compact formulation with numerical assessment and benchmarking," *Archives of Computational Methods in Engineering*, Vol. 10, No. 3, 2003, pp. 216–296.

[23] Carrera, E. and Giunta, G., "Refined beam theories based on a unified formulation," *International Journal of Applied Mechanics*, Vol. 2, No. 1, 2010, pp. 117–143, DOI: 10.1142/S1758825110000500.

[24] Carrera, E., Giunta, G., and Petrolo, M., *Beam Structures: Classical and Advanced Theories*, John Wiley & Sons, 2011, DOI: 10.1002/9781119978565.

[25] Carrera, E., Giunta, G., Nali, P., and Petrolo, M., "Refined beam elements with arbitrary cross-section geometries," *Computers and Structures*, Vol. 88, No. 5–6, 2010, pp. 283–293, DOI: 10.1016/j.compstruc.2009.11.002.

[26] Carrera, E., Petrolo, M., and Zappino, E., "Performance of CUF approach to analyze the structural behavior of slender bodies," *Journal of Structural Engineering*, Vol. 138, No. 2, 2012, pp. 285–297, DOI: 10.1061/(ASCE)ST.1943-541X.0000402.

[27] Carrera, E., Petrolo, M., and Nali, P., "Unified formulation applied to free vibrations finite element analysis of beams with arbitrary section," *Shock and Vibrations*, Vol. 18, No. 3, 2011, pp. 485–502, DOI: 10.3233/SAV-2010-0528.

[28] Carrera, E., Petrolo, M., and Varello, A., "Advanced Beam Formulations for Free Vibration Analysis of Conventional and Joined Wings," *Journal of Aerospace Engineering*, Vol. 25, No. 2, 2012, pp. 282–293, DOI: 10.1061/(ASCE)AS.1943-5525.0000130.

[29] Carrera, E. and Petrolo, M., "On the Effectiveness of Higher-Order Terms in Refined Beam Theories," *Journal of Applied Mechanics*, Vol. 78, No. 3, 2011, DOI: 10.1115/1.4002207.

[30] Carrera, E. and Petrolo, M., "Refined Beam Elements with only Displacement Variables and Plate/Shell Capabilities," *Meccanica*, Vol. 47, No. 3, 2012, pp. 537–556, DOI: 10.1007/s11012-011-9466-5.

[31] Carrera, E. and Petrolo, M., "Refined One-Dimensional Formulations for Laminated Structure Analysis," *AIAA Journal*, Vol. 50, No. 1, 2012, pp. 176–189, DOI: 10.2514/1.J051219.

[32] Carrera, E., Maiarú, M., and Petrolo, M., "Component-Wise Analysis of Laminated Anisotropic Composites," *International Journal of Solids and Structures*, Vol. 49, 2012, pp. 1839–1851, DOI: 10.1016/j.ijsolstr.2012.03.025.

[33] Euler, L., *De curvis elasticis*, Lausanne and Geneva: Bousquet, 1744.

[34] Timoshenko, S. P., "On the transverse vibrations of bars of uniform cross section," *Philosophical Magazine*, Vol. 43, 1922, pp. 125–131.

[35] Tsai, S. W., *Composites Design*, Dayton, Think Composites, 4th ed., 1988.

[36] Reddy, J. N., *Mechanics of laminated composite plates and shells. Theory and Analysis*, CRC Press, 2nd ed., 2004.

[37] Oñate, E., *Structural Analysis with the Finite Element Method: Linear Statics, Volume 1*, Springer, 2009.

[38] Bathe, K. J., *Finite element procedure*, Prentice hall, 1996.

Tables

	$u_z \times 10^3$ [m]	DOFs
Analytical Methods		
BS	-2.671	-
PS	-3.059	-
Classical Beam Theories		
EBBT	-1.827	279
TBT	-2.117	279
TE		
$N = 3$	-2.514	930
$N = 5$	-2.629	1953
$N = 7$	-2.738	3348
$N = 9$	-2.890	5115
CW		
4 L9, Fig. 7a	-3.639	2883
8 L9, Fig. 7b	-3.639	4743
MSC/NASTRAN©		
SOLID	-3.815	76050

Table 1 Displacement values, u_z, at the loaded point and number of degrees of freedom of each model, two-stringer spar.

	P [N]	q [N/m]
*all values are multiplied $\times 10^{-4}$		
Analytical Methods		
BS	3.192	-1.064
PS	3.192	-1.064
Classical Beam Theories		
EBBT	1.993	-0.274
TBT	1.993	-0.274
TE		
$N = 3$	2.434	-0.665
$N = 5$	2.350	-0.561
CW		
4 L9, Fig. 7a	2.833	-1.034
8 L9, Fig. 7b	2.739	-1.035
MSC/NASTRAN©		
SOLID	2.713	-1.036

Table 2 Axial load in the upper stringer, P, at $y = 0$ and mean shear flow on the sheet panel, q, at $y = \frac{L}{2}$, two-stringer spar.

	$u_z \times 10^3$ [m]	P [N]	DOFs
SOLID #1	−3.785	2.577	2805
SOLID #2	−3.815	2.713	76050
SOLID #3	−3.862	2.709	198246

Table 3 Displacement values, u_z, at the loaded point, axial load in the upper stringer, P, at $y = 0$ and number of degrees of freedom of SOLID models, two-stringer spar.

	$u_z \times 10^3$ [m]	DOFs
Analytical Methods		
BS	−1.309	-
PS	−1.471	-
Classical Beam Theories		
EBBT	−1.325	279
TBT	−1.487	279
TE		
$N = 4$	−1.661	1395
$N = 6$	−1.707	2604
$N = 8$	−1.730	4185
CW		
5 L9	−1.846	3813
MSC/NASTRAN©		
SOLID	−1.857	72450

Table 4 Displacement values, u_z, at the center of the intermediate stringer and number of degrees of freedom, three-stringer spar.

	q_1 [N/m]	q_2 [N/m]	P_1 [N]	P_2 [N]	P_3 [N]
*all values are multiplied $\times 10^{-4}$					
Analytical Methods					
BS	−0.859	−1.095	2.574	0.730	−3.285
PS	−0.949	−1.118	2.847	0.507	−3.353
Classical Beam Theory					
EBBT	−0.305	−0.305	2.323	0.733	−2.766
TBT	−0.305	−0.305	2.323	0.733	−2.766
TE					
$N = 4$	−0.071	−0.902	3.208	0.081	−3.202
$N = 6$	−0.402	−1.006	2.997	0.727	−3.251
$N = 8$	−0.469	−1.052	2.916	0.639	−3.215
CW					
5 L9	−0.820	−1.150	2.495	0.633	−2.980
MSC/NASTRAN©					
SOLID	−0.816	−1.150	2.457	0.572	−2.781

Table 5 Axial loads in the stringers at $y = 0$ and mean shear flows on the sheet panels at $y = \frac{L}{2}$, three-stringer spar.

	q_1 [N/m]	q_2 [N/m]	q_3 [N/m]	q_4 [N/m]	P_1 [N]	P_2 [N]	P_3 [N]	P_4 [N]	DOFs
*all values are multiplied $\times 10^{-3}$									
				CW					
8 L9	5.092	−5.173	−5.121	−16.624	23.313	−23.313	−26.211	26.211	6588
	(−0.032)	(0.005)	(0.033)	(−21.789)	(−5.839)	(5.839)	(−55.007)	(55.007)	(5952)
12 L9	4.969	−5.171	−4.966	−16.654	21.033	−21.033	−24.603	24.603	9036
	(−0.164)	(0.013)	(0.164)	(−21.841)	(−5.488)	(5.488)	(−51.143)	(51.143)	(8184)
20 L9	5.037	−5.145	−5.034	−16.654	20.286	−20.286	−23.767	23.767	13932
	(−0.061)	(0.010)	(0.092)	(−21.827)	(−5.235)	(5.235)	(−49.548)	(49.548)	(12648)
				MSC/NASTRAN©					
SOLID/SHELL	5.077	−5.200	−5.149	−16.651	21.670	−21.670	−24.660	24.660	22346
	(−0.381)	(0.293)	(−0.242)	(−21.530)	(−5.435)	(5.435)	(−51.765)	(51.765)	(22020)
SOLID	5.074	−5.104	−5.074	−16.368	20.166	−20.166	−22.942	22.942	115362
	(−0.071)	(0.011)	(0.071)	(−21.483)	(−5.163)	(5.163)	(−48.271)	(48.271)	(112200)

Table 6 Convergence of the CW models. Mean shear flows on the sheet panels at $y = \frac{L}{2}$, axial loads in the stringers at $y = 0$ and number of degrees of freedom. Rectangular wing box with rib at the tip. Results by models without rib are reported in brackets.

	q_1 [N/m]	q_2 [N/m]	q_3 [N/m]	q_4 [N/m]	P_1 [N]	P_2 [N]	P_3 [N]	P_4 [N]	DOFs
*all values are multiplied $\times 10^{-3}$									
				Analytical Methods					
BS	5.435	−5.435	−5.435	−16.304	32.609	−32.609	−32.609	32.609	-
PS	5.221	−5.221	−5.221	−16.518	31.325	−31.325	−33.893	33.893	-
				Classical Beam Theories					
EBBT	0	−1.701	0	−1.701	19.757	−19.757	−19.757	19.757	306
TBT	0	−1.701	0	−1.701	19.757	−19.757	−19.757	19.757	306
				TE					
$N = 4$	4.470	−4.603	−4.470	−14.142	23.197	−23.197	−26.418	26.418	1530
	(4.769)	(−4.897)	(−4.769)	(−13.848)	(23.167)	(−23.167)	(−26.448)	(26.448)	(1395)
$N = 6$	4.848	−4.579	−4.846	−14.218	23.529	−23.523	−27.567	27.556	2856
	(5.654)	(−5.329)	(−5.655)	(−13.467)	(23.404)	(−23.404)	(−27.684)	(27.686)	(2604)
$N = 8$	4.647	−5.148	−4.894	−16.240	23.803	−23.837	−26.579	26.722	4490
	(1.478)	(−1.204)	(−1.478)	(−20.060)	(1.555)	(−1.531)	(−48.968)	(48.976)	(4185)
				CW					
	5.037	−5.145	−5.034	−16.654	20.286	−20.286	−23.767	23.767	13932
	(−0.061)	(0.010)	(0.092)	(−21.827)	(−5.235)	(5.235)	(−49.548)	(49.548)	(12648)
				MSC/NASTRAN©					
SOLID/SHELL	5.077	−5.200	−5.149	−16.651	21.670	−21.670	−24.660	24.660	22346
	(−0.381)	(0.293)	(−0.242)	(−21.530)	(−5.435)	(5.435)	(−51.765)	(51.765)	(22020)
SOLID	5.074	−5.104	−5.074	−16.368	20.166	−20.166	−22.942	22.942	115362
	(−0.071)	(0.011)	(0.071)	(−21.483)	(−5.163)	(5.163)	(−48.271)	(48.271)	(112200)

Table 7 Mean shear flows on the sheet panels at $y = \frac{L}{2}$, axial loads in the stringers at $y = 0$ and number of degrees of freedom. Rectangular wing box with rib at the tip. Results by models without rib are reported in brackets.

	Full Model		No Ribs Case		Open Mid-bay Case	
	$u_z \times 10^2$ [m]	DOFs	$u_z \times 10^2$ [m]	DOFs	$u_z \times 10^2$ [m]	DOFs
			MSC/NASTRAN©			
SOLID/SHELL	1.412	100026	3.051	89400	1.963	89621
			Classical Beam Theories			
EBBT	0.464	495	0.464	495	0.464	495
TBT	0.477	495	0.477	495	0.477	495
			TE			
$N = 3$	0.793	1650	0.794	1650	0.873	1650
$N = 5$	1.108	3465	1.203	3465	1.500	3465
$N = 7$	1.251	5940	2.158	5940	1.745	5940
$N = 9$	1.325	9075	2.649	9075	1.836	9075
			CW			
	1.397	10750	2.981	10560	1.919	10446

Table 8 Displacement values, u_z, at the loaded point and number of degrees of freedom for the considered structural configurations of the three-bay wing box.

	Full Model		No Ribs Case		Open Mid-bay Case	
Model	σ_{yy} [MPa]	σ_{yz} [MPa]	σ_{yy} [MPa]	σ_{yz} [MPa]	σ_{yy} [MPa]	σ_{yz} [Pa]
SOLID/SHELL	80.598	120.730	178.147	155.368	123.841	115.351
CW LE	80.404	120.603	177.018	151.876	118.684	115.810

Table 9 Stress components, σ_{yy} at $[b, \frac{l}{2}, -\frac{h_2}{2}]$ and σ_{yz} at $[b, \frac{l}{2}, 0]$, of the different structural configurations of the three-bay wing box.

Figures

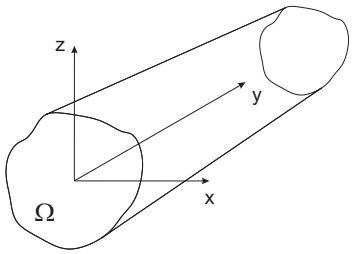

Fig. 1 Coordinate frame of the beam model.

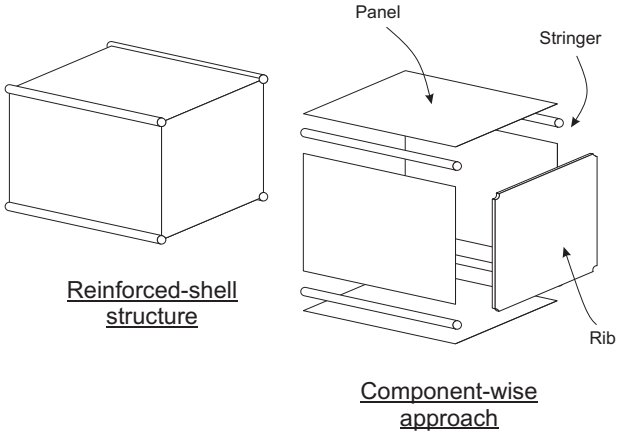

Fig. 2 Component-wise approach.

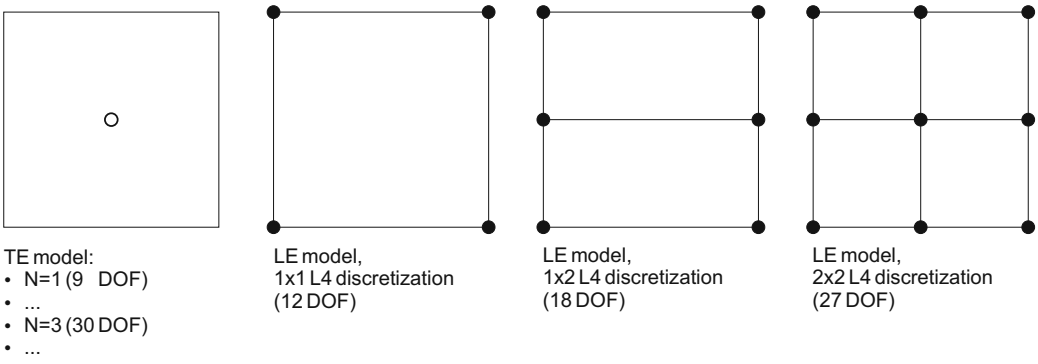

Fig. 3 Differences between the TE and LE models.

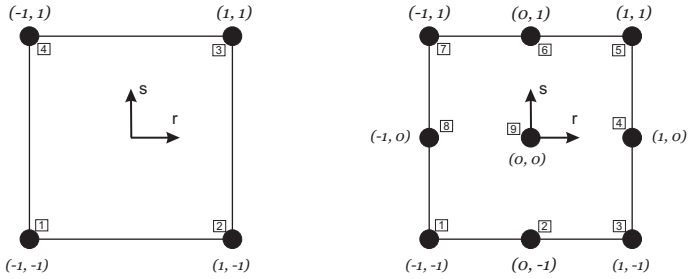

(a) Four-point element, L4 (b) Nine-point element, L9

Fig. 4 Cross-section L-elements in natural geometry.

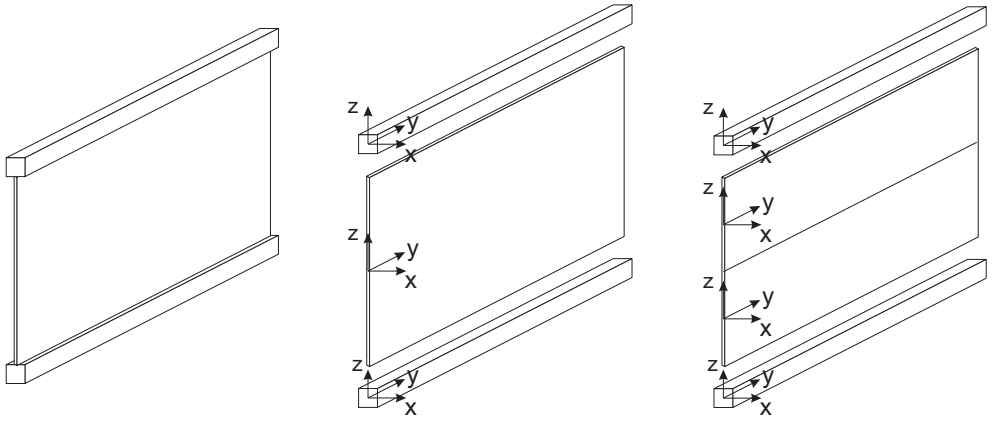

(a) Two-stringer spar

(b) Each of the two stringers and the panel are modelled with one LE 1D element

(c) The panel is modelled with two 1D LE elements

Fig. 5 CW approach through LE elements.

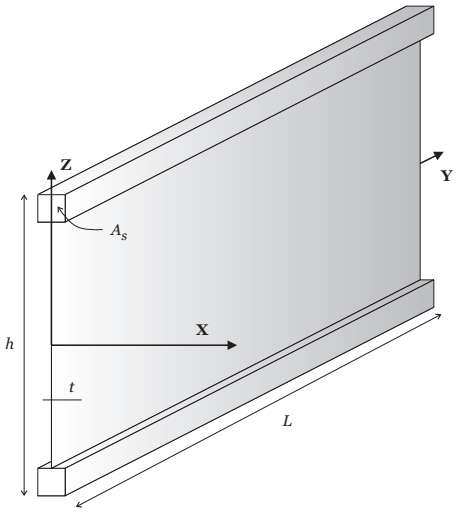

Fig. 6 Two-stringer spar.

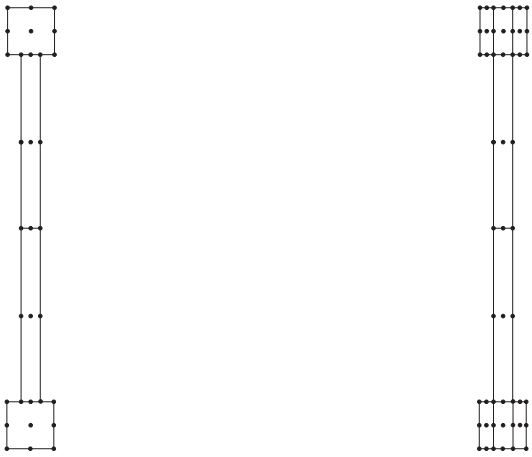

(a)
4 L9

(b)
8 L9

Fig. 7 Cross-section L9 distributions for the LE models of the two-stringer spar.

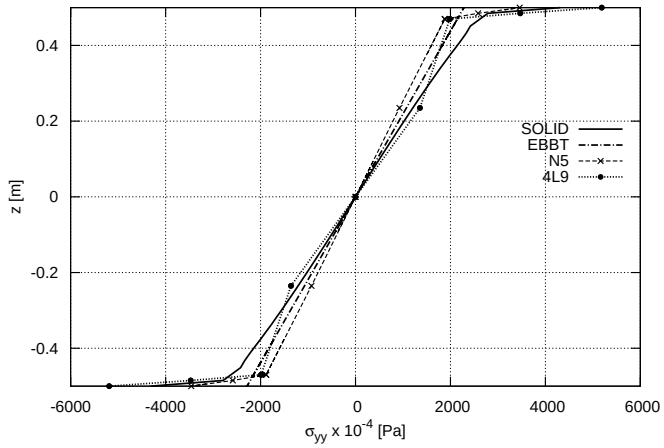

(a) σ_{yy} vs. z at $x = y = 0$

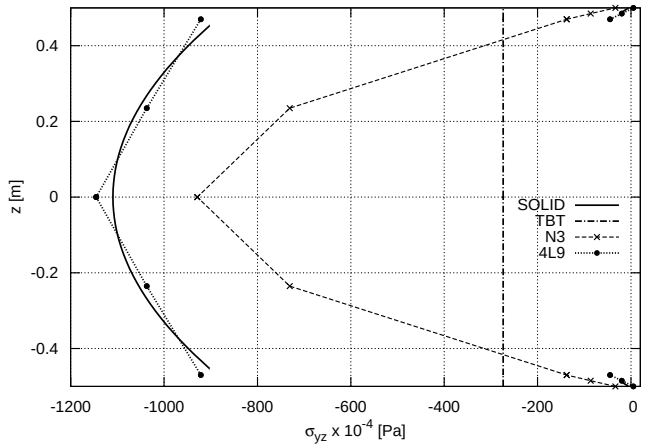

(b) σ_{yz} vs. z at $x = 0$, $y = \frac{L}{2}$

Fig. 8 Axial stress, σ_{yy}, and shear stress, σ_{yz}, versus the z-axis, two-stringer spar.

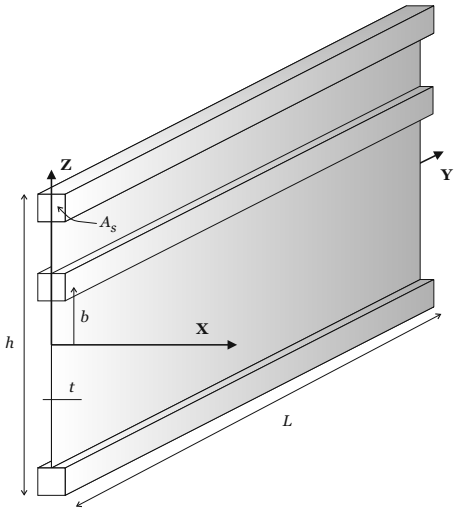

Fig. 9 Three-stringer spar.

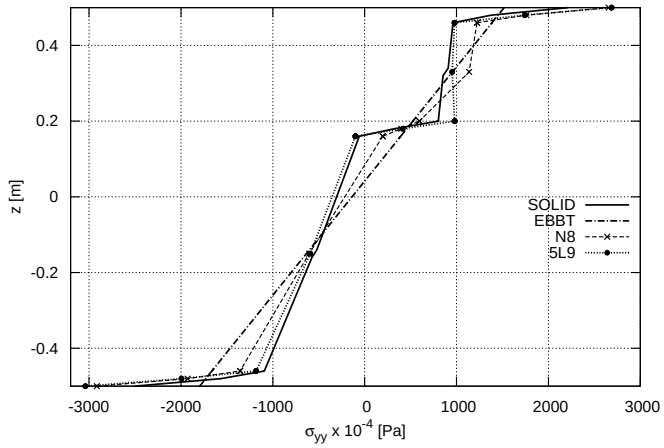

(a) σ_{yy} vs. z at $x = y = 0$

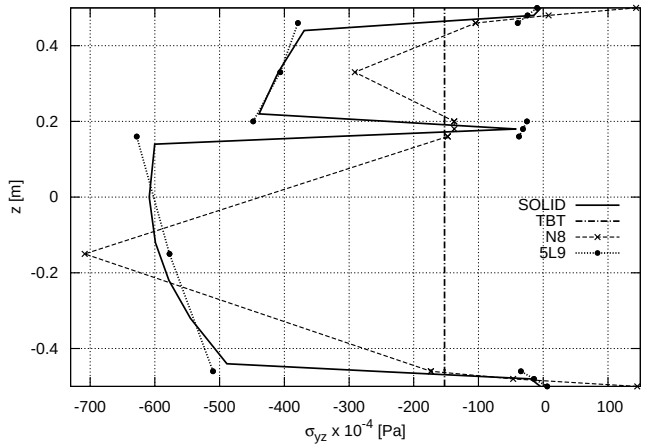

(b) σ_{yz} vs. z at $x = 0$, $y = \frac{L}{2}$

Fig. 10 Axial stress, σ_{yy}, and shear stress, σ_{yz}, versus the z-axis, three-stringer spar.

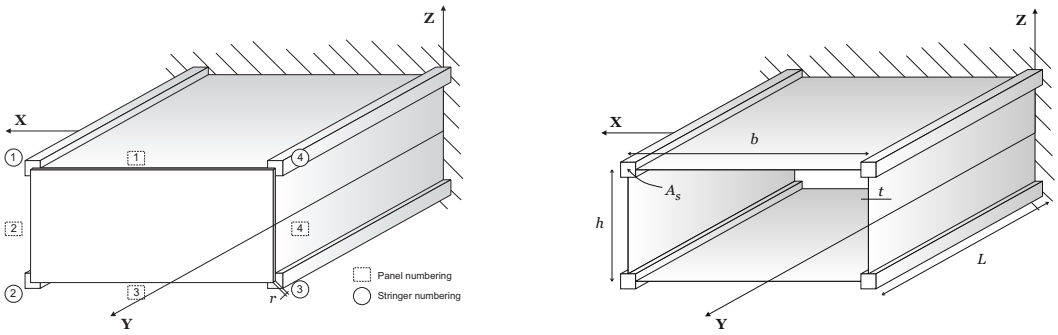

(a) (b)

Fig. 11 Rectangular wing boxes.

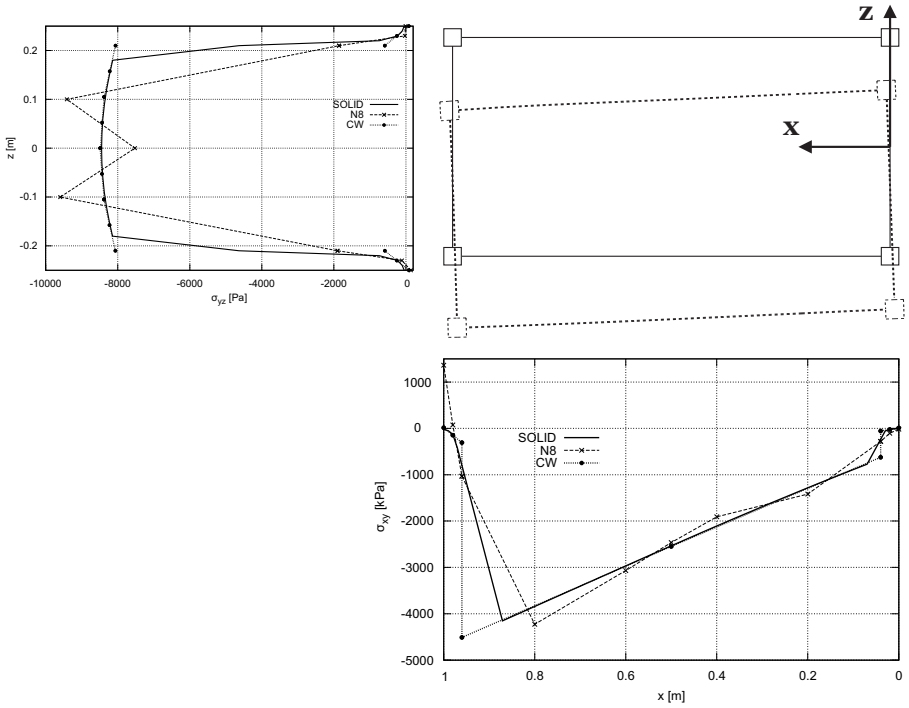

Fig. 12 σ_{yz} versus the z-axis at $x = b$, $y = \dfrac{L}{2}$ and σ_{xy} versus the x-axis at $z = -\dfrac{h}{2}$, $y = \dfrac{L}{2}$. Deformed tip cross-section by eighth-order TE model is drawn (amplifying factor $\times 10$), rectangular wing box with rib at the tip.

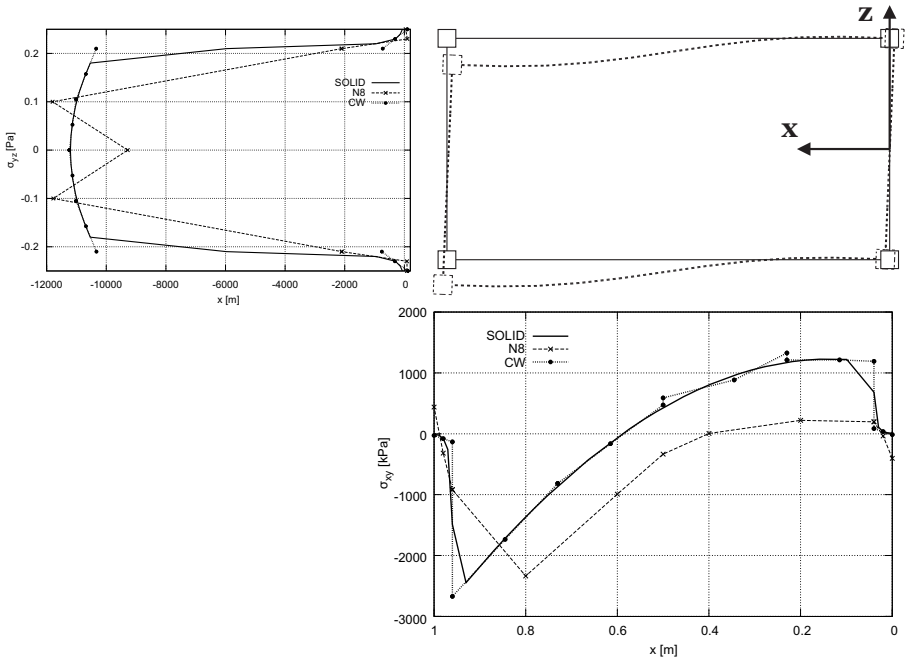

Fig. 13 σ_{yz} **versus the** z**-axis at** $x = b$**,** $y = \dfrac{L}{2}$ **and** σ_{xy} **versus the** x**-axis at** $z = -\dfrac{h}{2}$**,** $y = \dfrac{L}{2}$**. Deformed tip cross-section by eighth-order TE model is drawn (amplifying factor** $\times 10$**), rectangular wing box with no rib.**

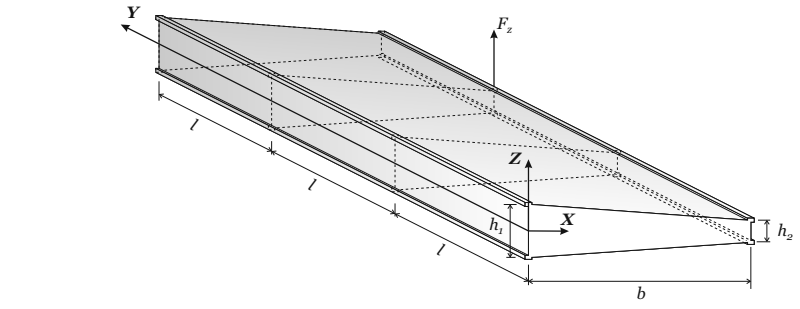

(a) Full model

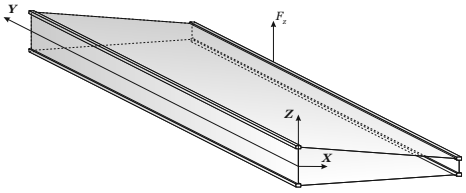

(b) No ribs case

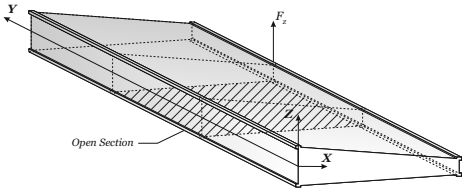

(c) Full model with open mid-bay

Fig. 14 Different structural configurations of the three-bay wing box.

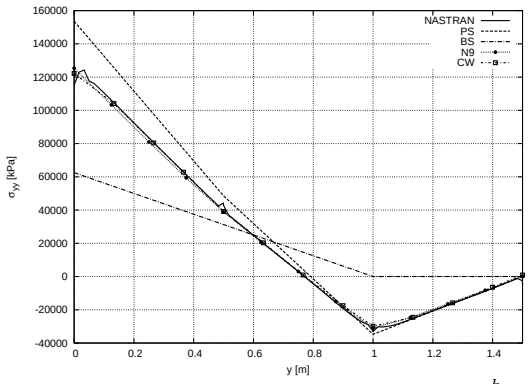

(a) Bottom right spar cap; σ_{yy} at $x = b$, $z = -\frac{h_2}{2}$

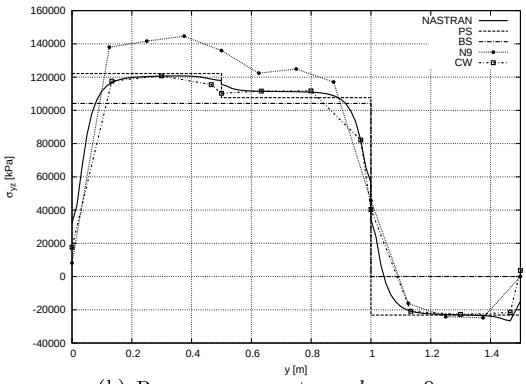

(b) Rear spar; σ_{yz} at $x = b$, $z = 0$

Fig. 15 Stress components distribution along the wing span. Comparison of analytical, MSC/NASTRAN© and CUF models, full model of the three-bay wing box.

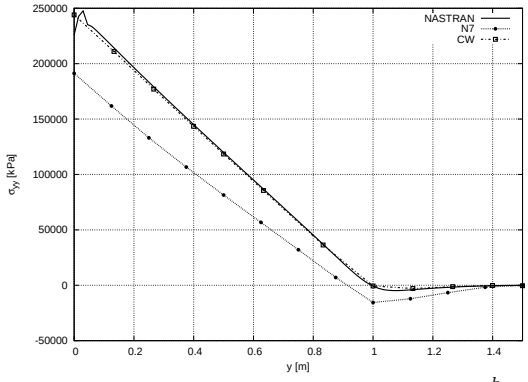

(a) Bottom right spar cap; σ_{yy} at $x = b$, $z = -\frac{h_2}{2}$

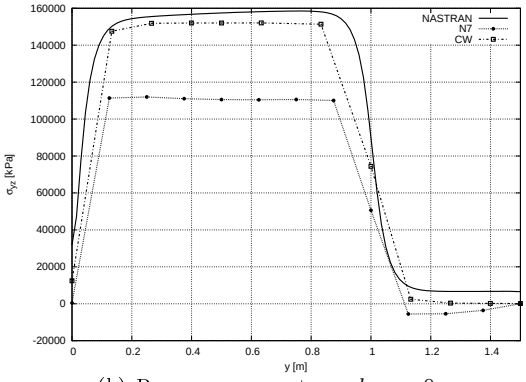

(b) Rear spar; σ_{yz} at $x = b$, $z = 0$

Fig. 16 Stress components distribution along the wing span. Comparison of MSC/NASTRAN© and CUF models, three-bay wing box with no ribs.

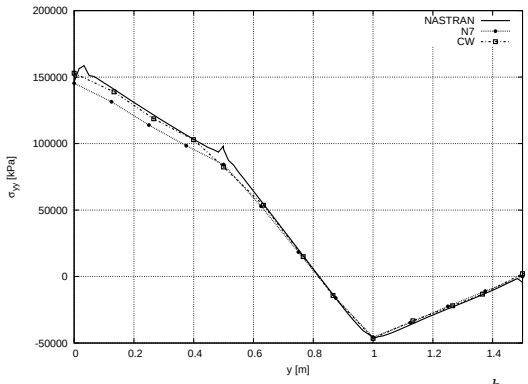

(a) Bottom right spar cap; σ_{yy} at $x = b$, $z = -\frac{h_2}{2}$

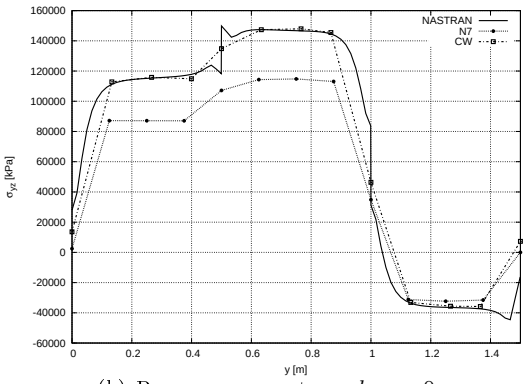

(b) Rear spar; σ_{yz} at $x = b$, $z = 0$

Fig. 17 Stress components distribution along the wing span. Comparison of MSC/NASTRAN© and CUF models, three-bay wing box with open mid-bay.